Tribology International 42 (2009) 475–490

Contents lists available at ScienceDirect

Tribology International

journal homepage: www.elsevier.com/locate/triboint

An investigation into the effect of train curving on wear and contact stresses of wheel and rail

Xuesong Jin *, Xinbiao Xiao, Zefeng Wen, Jun Guo, Minhao Zhu

State Key Laboratory of Traction Power, Southwest Jiaotong University, Chengdu, Sichuan 610031, China

ARTICLE INFO

Article history:
Received 24 November 2006
Received in revised form
3 August 2008
Accepted 20 August 2008
Available online 15 October 2008

Keywords:
Rail wear
Contact stress
Railway vehicle
Curved track
Rolling contact mechanics
Structure dynamics

ABSTRACT

Some important papers concerning the studies on rail wear and wheel/rail contact stresses are briefly reviewed. The present paper utilizes a numerical method to analyze the effect of railway vehicle curving on the wear and contact stresses of wheel/rail. The numerical method considers a combination of Kalker's non-Hertzian rolling contact theory, a material wear model and a vertical and lateral coupling dynamics model of the vehicle/track. In the analysis, the important factors influencing on the wear and the contact stresses are, respectively, the curving speed, the curved track super-elevation and the rail cant. Compared to the present model, some concerned models and results in the published papers are in detail discussed. Through the detailed numerical analysis, it is found that the difference between the normal loads of the left and right of the wheelset increases linearly with increasing the vehicle curving speed. The material wear volume per length along the rail running surface has a tendency to grow. However, the variation of the maximum normal contact stress has a large fluctuation as the curving speed increases. The increase of the maximum contact stress depends greatly on not only the normal load but also the profiles of the wheel/rail. Increasing the track super elevation efficiently lowers the normal load difference of the left and right of the front wheelset, and the contact stresses and the wear. The rail cant has a great influence on the low rail wear of the curve track. An increase in rail cant results in a great increase in the low rail wear of the curved track, and a decrease in the outside rail wear. These conclusions are very useful in the maintenance of the track.

1. Introduction

The wear and rolling contact fatigue of wheels and rails cost China railways about 1.2 billions US dollars per year. The wear and fatigue occur predominantly on sharp curved tracks, joint rails and turnouts [1,2]. When a wheel rolls over a rail with a large slide, a large amount of material on the wheel or rail running surface is removed due to larger contact stresses and high temperature [3]. Fig. 1a and b illustrates, respectively, severe side wear and severe corrugation occurred on high curved rails. Such wear causes the great change of rail profile and, therefore, strongly affects the running behavior of railway vehicles, such as motion stability, riding comfort and derailment safety. The wear amount and the present shape of the rail in service are the key criteria for rail replacement at railway sites. However, the wear is often utilized to extend the use life of the rails which have small cracks on their running surfaces at railway sites. As well known, the rail has two types of damage: cracks and wear. Proper wear rate occurring on the rail running surface is able to eliminate small existing cracks or suppress the growth of existing cracks efficiently [4]. According to the mechanism many railway companies on the world developed the optimum techniques of rail grinding [5–7]. For instance, MRS in Brazil applied the advanced technique of rail grinding to the maintenance of the heavy haul track, and the use life of rails used in the heavy haul increased doubly [8]. Therefore, railway companies are much concerned with the studies and treatment of rail wear. Rail wear studies are very complicated, and involve many subjects, such as structural coupling dynamics of railway vehicle and track, rolling contact mechanics, tribology, metallurgy, and numerical method.

In the past, many papers on wheel/rail wear were published. In 1976, using Amsler testing machine of two rollers, Bergley made an investigation into the wear of wheel flanges against the sides of the rails, caused by rolling/sliding contacts sustaining high cyclic stresses at low slide/roll ratios [9]. He concluded that the severe wear of contacts at low slide/roll ratios is caused by high resolved cyclic stresses that result in continual plastic deformation of the surface layers. Using the same testing facility, three wear regimes of wheel/rail steels in rolling/sliding contact were identified by Bolton et al. [10,11]. The characteristic of wear modes within these

* Corresponding author. Tel.: +86 28 87634355; fax: +86 28 87600868.
E-mail address: xsjin@home.swjtu.edu.cn (X. Jin).

0301-679X/$ - see front matter © 2008 Elsevier Ltd. All rights reserved.
doi:10.1016/j.triboint.2008.08.004

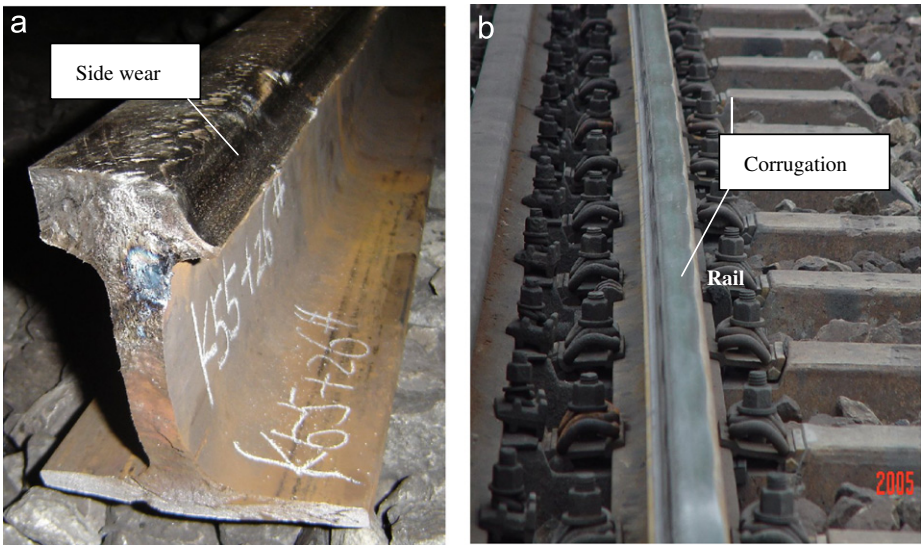

Fig. 1. (a) Curved rail side wear and (b) curved rail corrugation.

regimes, referred to as types I, II and III, was determined through metallurgical examination. Relations between the wear rates and test contact parameters, for wear types I and II, can be presented by mathematical expression. It was found that the wear modes occurred in side-worn rail on curved track correlated with laboratory wear types II and III to the extent that the laboratory test offers a prediction of the wear status of rail in service [12]. Tyfour et al. [13] made an investigation into the steady-state wear behavior of pearlitic rail steel after a certain number of rolling–sliding cycles through test in detail. Also the effect of strain hardening and unidirectional plastic strain accumulation on the wear behavior was studied. The test result shows that the start of the steady-state wear rate coincides with the cessation of plastic strain accumulation and additional strain hardening, namely, the steady-state wear rate is established when the material with the same history of strain hardening and accumulated unidirectional plastic strain reaches the surface and the unidirectional plastic strain limit to failure is reached. In their results it was found that the rates of strain accumulation and strain hardening present maxima at the beginning of the rolling/sliding process, and decrease in non-linear fashion to stop after a certain number of cycles. Muster et al. [14] observed and analyzed the effect of different grades of rail steel in service on the resistance to wear and fatigue damage. Tournay and Mulder [15] analyzed the transition from the wear to stress regime of the rails in service. They found that tighter gauge tolerances led to rail crown grinding producing tighter contact bands, and improved vehicle tracking properties. The concentrated contact formed on the wheel tread enhancing hollow wear band. Since the lateral excursions of the wheelsets often occur outside, the deep hollow wear band, small contact areas, high contact stresses and large longitudinal creepages as a result of the large instant radius difference generated on the wheelsets, often form. This can cause high longitudinal material flow, shelling and checking in the rails. Ueda et al. [16] clarified the effects of carbon content on the rolling contact wear in pearlitic steels through a detailed two-cylinder rolling contact wear test, using pearlitic steels with a carbon content ranged from 0.8 to 1.0 mass%. They obtained conclusions as follows: (1) the wear resistance of pearlitic rail steels improves as carbon content and rolling contact surface hardness increase, and the rolling contact surface hardness is a main factor affecting the wear; (2) the rolling contact surface hardness increases due to raising the working-hardening rate of the rolling contact surface as carbon content increases. That is because an increase in the cementite density increases the amount of dislocation in the matrix ferrite and promotes the grain refinement of the matrix ferrite. Therefore, the matrix ferrite is strengthened. Through experimental examinations of the tractive rolling contact between rail and wheel using two-roller test machine, Deters and Proksch [17] found that the wear volume rise turned out to be proportional to the increase of the acting pressure and the creepage between the two rollers. An increase in the circumferential speed of the test rollers caused a reduction in the wear volume. A significant wear decrease at the driven roller modeling rail could be achieved by periodically reversing the direction of the acting traction force.

Actually, the wear and rolling contact fatigue of wheel/rail depend greatly on their profiles and contact surface status, the geometry sizes of track and dynamical behavior of railway vehicle coupled with the track. Their numerical analysis needs the power and efficient numerical method considering the factors mentioned above. Such a numerical method can help identify the risk of severe or catastrophic wear resulting from increased train speeds and axle loads, and determine more efficient maintenance schedules for track and rolling stock [18]. Shen et al. [19] numerically analyzed the influence of rail lubrication on freight car wheel/rail wear rates. Their numerical model considered a C_{60} freight car of China with two sets of standard 3-piece trucks, called "TRUCK 8" under the condition of steady-state curving through a rigid curved track. The steady-state curving indicates that the accelerations of the system in the calculation were neglected. Only the equations for a single-track/half-car body were solved in order to reduce the numerical computation. Rail lubrication was simulated through changing the friction coefficient between the wheels/rails. The non-linear creep forces in the Hertzian elliptical contact areas of the wheels/rails were calculated with the model put forward by Shen et al. [20]. The numerical results indicated that for the curved tracks with radii less than 400 m, the wheel/rail wear rate, under lubrication, may be reduced to 40% of that without lubrication. Jendel [21] developed a wheel profile wear prediction tool based on a load collective concept, where time-domain dynamics simulation of the vehicle coupled with track was carried out based on actual

track data, measured rail profiles as well as pertinent conditions. In Jendel's calculation model, the vehicle model consisted of a full dynamic rigid multi-body model with a car-body, two bogie frames and four wheelsets connected by linear and non-linear suspension elements. The track was modeled as a mass following each wheelset with a degree of freedom in the lateral direction. Archard's wear model was used to calculate the material removal due to wear [22]. To verify the prediction tool, they made comparisons between the simulated and measured wheel profiles for a total running distance of about 200,000 km, as well as between four scalar wear measures: flange thickness, flange height, flange inclination and the decrease in area between successive profiles. The comparisons showed a good agreement. Ref. [23] declared a method for the computation of the rail surface degradation in a curved track where the major surface degradation phenomenon is, actually, a combination of wear and plastic deformation. In the numerical analysis of the wheel/rail in rolling contact, the normal pressure was calculated with the modified Winkler method [24], and calibrated with the results obtained by FEM modeling of the wheel/rail in contact with elastic/plastic deformation [25]. A tangential Winkler model that includes the effect of neighbouring cells was used to calculate the elastic tangential stress and displacement field. In Archard's wear model used to calculate the material removal due to wear, the friction coefficient and wear coefficient were determined in advance using pin on disk tests [26]. Two point contacts occur easily between the leading wheelsets and the high rails of sharp curved track during the curving of trains. Such two point contacts cause severe side-wear of the rails. So, a typical two-point contact in a sharp curve was analyzed and discussed by Telliskivi and Olofsson [25]. Enblom and Berg [27] analyzed the wheel profile development due to wear-influence of disk braking and contact environment. Their wear prediction model is the same as that Jendel used. Magel et al. [28] evaluated the comparative wear performance of the new improved profile wheel against existing wheels through a numerical simulation of the wheel–rail interaction over 800 km of running by using a quasi-static curving model that was validated through a comparison with NUCARS predictions. Their prediction showed that the improved profile wheel reduced wheel flange wear by at least 25% when compared to the existing Amtrak Standard wheel profile. Shevtsov et al. [29] presented a numerical procedure for design of wheel profiles based on the function of rolling radii difference of left and right wheels of wheelset. Using the procedure the obtained new wheel profile can reduce wheel/rail wear without loss of the vehicle dynamic performance, which is validated through the analysis using ADAMS/Rail computational software.

In the present study, a numerical method is used to investigate the influence of a railway vehicle curving on rail wear and wheel–rail contact stresses. The method considers Kalker's three-dimensional rolling contact theory with non-Hertzian form, a material wear model, the vertical and lateral coupling dynamics of a half-railway vehicle and a curved track, and the contact geometry calculation of wheelset and track. Kalker's rolling contact theory [30] is introduced and modified [31] to calculate the frictional work density and the contact stresses in the Non-Hertzian contact areas between the wheels and rails. The material wear volume is calculated with the linear model of material wear related to the frictional work density [32,33]. A half-railway vehicle coupled with a complicated physical model of the track is considered in the dynamics simulation. The half vehicle has a two-axle bogie and doubled suspension systems. It was treated as a full dynamic rigid multi-body model. The model of the track by Zhai et al. [34] was introduced in the present work. Also the paper compares and discusses some concerned models and results in the published papers.

2. Model of rail wear calculation and contact stresses

2.1. General descriptions

Curved rail wear depends greatly on the profiles, materials and contact surface status of wheel and rail, train curving speed, and dynamical characteristics of railway vehicle and curved track. Under a given wheel load, the profiles and surface status of wheel and rail determine the wheel–rail contact stresses which affect the rail wear. Severe rail wear changes the profiles of wheel and rail much. The much changed profiles make railway vehicle tracking performance become very bad. The larger normal load and creep forces generate between the wheel and rail. The contact stresses, therefore, become larger. Such a situation easily destroys vehicles and track, especially, results in severe damage on the running surfaces of wheel and rail. The vehicle curving behavior is intimately related to the dynamical characteristics of the vehicle and the track. In addition, the physical properties of wheel and rail materials much affect the rate of material wear and crack growth on the rail running surface. The influences of the above factors are strongly coupled. It is very necessary that a complete and complicated model accounting for these factors is developed to predict the profile degradation of rail due to wear.

The present model is roughly depicted in Fig. 2 according to the above brief discussion on these factors. In Fig. 2, Y_{wi} and ψ_{wi} are, respectively, the lateral displacement and yaw angle of wheelset i, subscripts $i=1,\ 2$ denote the leading and trailing wheelsets considered in the calculation model, respectively, Y_{rk} is the lateral displacement of the rail head under wheel k, and subscript k is the number of the wheels in the model, δ_k and h_k are, respectively, the contact angle and the normal distance between wheel k and the rail. The selected ranges for i and k depend on the total numbers of the wheelsets in the calculation model. ξ_{jk} and P_{wrzk} are, respectively, the creepages and the vertical loads between the wheels and the rails, subscripts $j=1,\ 2,\ 3$ indicate, respectively, the longitudinal, lateral and normal directions, subscripts w and r denote, respectively, wheel and rail, z indicates the vertical direction of the track. f_{wk} denotes the frictional work density in the contact area under wheel k. Fig. 2 indicates a feedback process between the transient coupling dynamics of the vehicle and the curved track and long-term wear processes. In the analysis, a coupling dynamics model of the railway vehicle and the curved track is used to analyze the behavior of the vehicle and the track. Through the dynamics analysis, ξ_{jk}, P_{wrzk}, Y_{wi}, ψ_{wi} and Y_{rk} are obtained. Using the calculation model of wheel-rail contact geometry briefly discussed in the present paper later, and known Y_{wi}, ψ_{wi} and Y_{rk}, h_k and δ_k are found. ξ_{jk}, P_{wrzk}, h_k and δ_k will be used in the rolling contact calculation of the wheel/rail with Kalker's rolling contact theory. Through the rolling contact calculation, we obtain f_{wk}, the contact stresses, stick/slip areas, the wear volume, etc. Kalker's model of three-dimensional elastic bodies in rolling contact is introduced, and must be modified in such the rolling contact calculation of the wheel/rail systems, where the effect of the rail profile change on the dynamics and the contact is considered. If the frictional work density on the contact area is known, the wear depth on the running surface is determined using the material wear model by Clayton et al. [32,33]. So, using the known wear depth at the present step, the existing rail initial profile can be updated for the next loop calculation. After such repeated loop calculations the accumulated material wear and its distribution on the rail head are obtained. In each step calculation, the contact stresses, the stick/slip areas, the slip distribution in the contact area, etc. are also determined.

It should be noted that, for the introduced rail wear model, effect of material working-hardening, due to repeat rolling and press of wheels, on the wear is neglected.

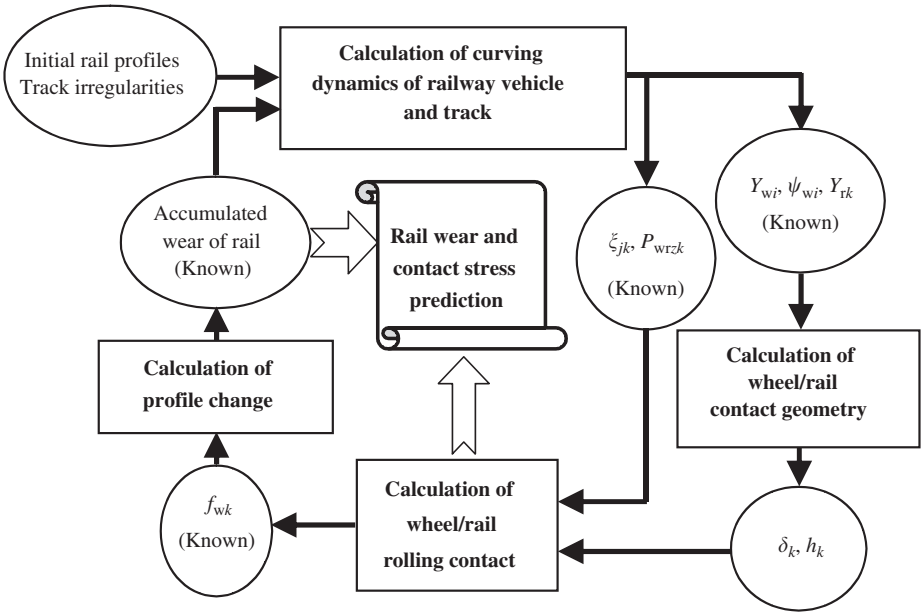

Fig. 2. A general description of curved rail wear model.

2.2. Model of railway vehicle and curved track

At railway sites, severe wear usually occurs at sharp curved tracks. In the present model of railway vehicle and track, a half vehicle and a curved track with radius $R_0 = 800$ m, were taken into consideration. The curved track has the circle curve length $l_c = 200$ m, the transient curve length $l_{ct} = 120$ m, the track gauge $d_t = 1435$ mm, the super-elevation $h_t = 120, 150, 180$ mm, the rail cant $\alpha_t = 1/20, 1/30, 1/40$, and the sleeper pitch $l_0 = 600$ mm. The curving speed of the vehicle is selected as $v = 80, 100, 120$ km/h, respectively. The half vehicle curving is shown in Fig. 3. The calculation model of the half vehicle and the curved track, shown in Fig. 3, is described with Fig. 4a and b. In the figures the coordinate system X–Y–Z is the Cartesian system and an inertial one. The X-axis is in the moving direction of the vehicle, Z-axis in the vertical and down direction, and Y-axis in the lateral direction of the track, pointing to the right side of the track.

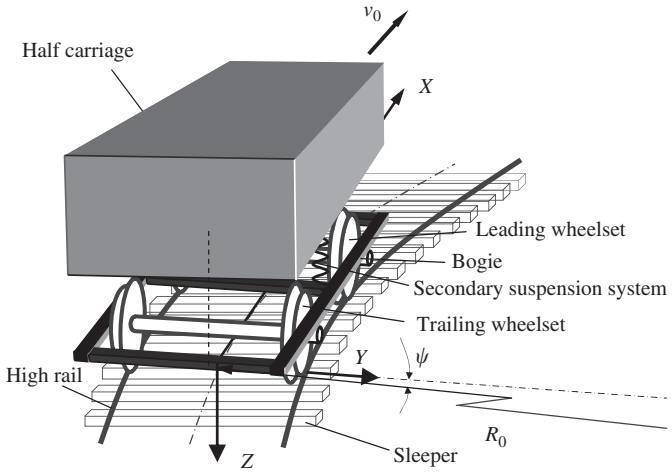

Fig. 3. A half vehicle passing a curved track.

2.2.1. Vehicle model description

From Fig. 4, it is obvious that the half vehicle is treated as a full dynamic rigid multi-body model. The variables Z, Y, ϕ and θ with subscripts indicate, respectively, the vertical displacement, the lateral displacement, the rolling angle and the pitching angle of the concerned components of the vehicle. K and C with subscripts stand for the coefficients of the equivalent spring stiffness and the equivalent damper, respectively. The equivalent springs and the equivalent dampers are used to replace the connections between the components of the half vehicle and the curved track. M_c is the mass of the half carriage. In order to present the numerical results clearly and conveniently, the left and right wheels of the leading wheelset are numbered with 1 and 2, respectively, and the corresponding wheels of the trailing wheelset numbered with 3 and 4. The leading and trailing wheelsets are numbered by 1 and 2, respectively. It should be noted that since the half vehicle is considered in the dynamics analysis it cannot be balanced when it runs on the track. Therefore, the pitching and yaw motions of the carriage must be neglected, namely, let $\theta_c = 0$ and $\psi_c = 0$ always, as shown in Fig. 4. The accelerations of the centers of all the components of the half vehicle are assumed to be zero in the longitudinal direction. The flexibility of the components of the vehicle is ignored.

2.2.2. Track model description

The track, except for the rails, is also treated as a dynamic rigid multi-body model. The calculation model of the track used in Ref. [34] is introduced in the present paper. Due to considering the half vehicle passing through the curved track, the four wheels of the same bogie interact with the two side rails of the track through the axle and the rails. Each rail is modeled by an Euler beam. The calculation length of the rails is 36 m. The two ends of the calculation rails are hinged (discussed later). The vertical and lateral bending deformations and twisting of the rails are taken into account. The longitudinal deformation and the cross influence of the vertical and lateral bending and twisting deformations of the rails are ignored. Using the Rayleigh–Ritz method, the fourth-order partial differential equations of the rail are converted into second-order ordinary equations [35,36]. The second-order ordinary equations are constituted based on the

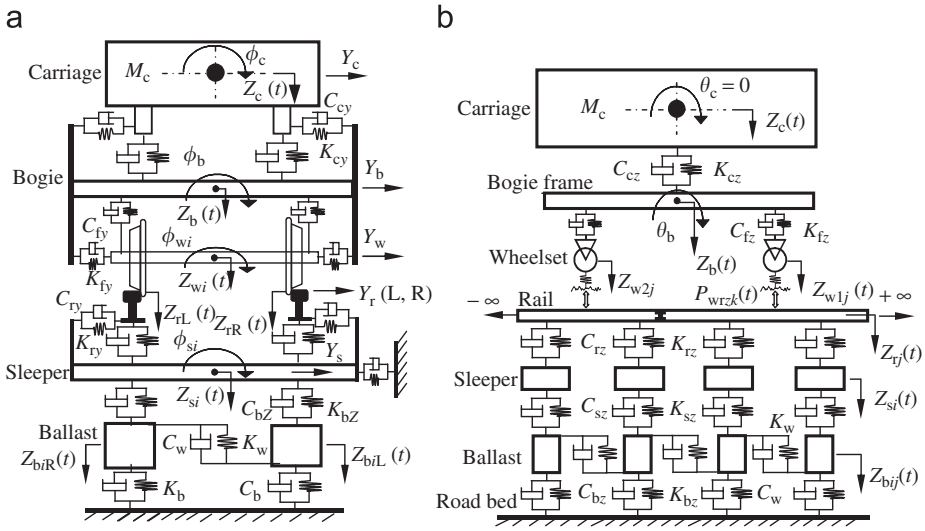

Fig. 4. (a) Elevation of a half passenger car coupled with a curved track and (b) side elevation.

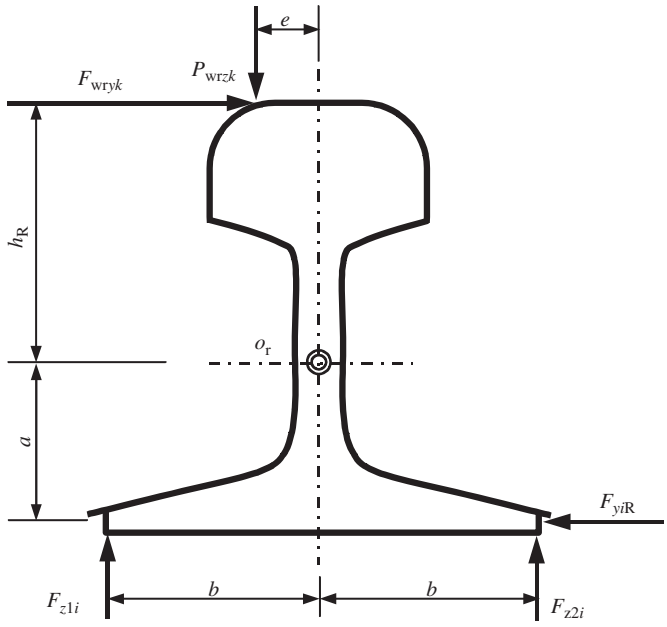

Fig. 5. Rail force diagram.

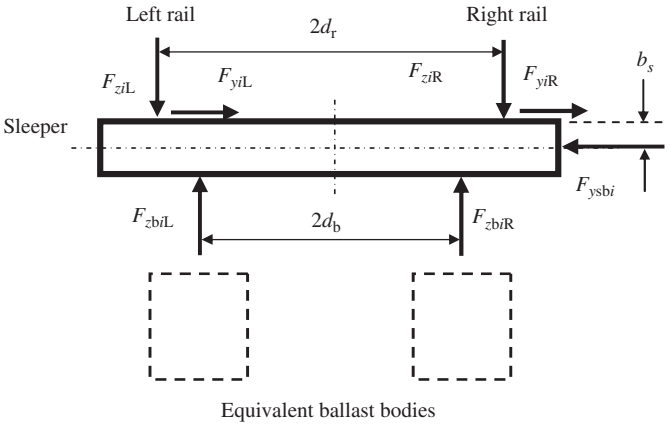

Fig. 6. Sleeper force diagram.

superposition principle of beam theory. The modal shape functions from the first to the 120th are used.

In the vertical and lateral plane of the track, the force diagrams of the right rail and the sleeper i are, respectively, illustrated with Figs. 5 and 6. In Figs. 5 and 6, the point o_r is the torsional center of the rail; P_{wrzk} and F_{wryk} are, respectively, the vertical and lateral forces of the wheel/rail; e is the distance from the contact point to the central line of the rail; (F_{z1i}, F_{z2i}, F_{yiR}) or (F_{ziR}, F_{yiR}, F_{ziL}, F_{yiL}) are the equivalent forces between the rail and the sleeper through the fastening system, which is replaced with the equivalent spring and the equivalent damper; (F_{zbiL}, F_{zbiR}) are the vertical forces between the sleeper and the left and right ballast bodies; F_{ysbi} is the lateral force on the sleeper by the ballast bed. The forces shown in the figures are related to the motion of the rails, the sleepers and the ballast bed, and the equivalent springs and dampers among them. The sleepers are treated as rigid bodies. Their vertical and lateral motions and rollings are considered. Since only the vertical motion of the equivalent ballast bodies is taken into consideration in the calculation model, the lateral restraint of the sleeper by the ballast bed is replaced by an equivalent spring and a damper in the lateral direction. One of their ends is connected to the end of the sleeper, and the other end is assumed to be fixed to the ground, as shown in Fig. 4a.

Since the ballast bed is piled with small stones with geometry and boundary irregularities, it is very difficult to completely characterize the ballast bed with any existing mathematical model so far. It is a very complicated research project related to non-linear physical properties of material and multi-bodies contacts. Fig. 7 shows a very simplified model used as a very crude approximation for the ballast bed considered in the present study. The ballast bed is replaced with the equivalent rigid ballast bodies. The vertical and shear springs and dampers are equivalently used to connect the neighbouring bodies, K_w and C_w, as shown in Fig. 4. Considering equivalent ballast bodies A and B in the bed, their calculation model is shown in the right side of Fig. 7. F_{zfiL}, F_{zriL}, F_{zfiR}, F_{zriR} and F_{ziLR} are the vertical shear forces between the neighbouring ballast bodies, F_{zgiL} and F_{zgiR} are the vertical forces between the ballast bodies and the road-bed (ground). In the dynamic analysis, only the vertical motion of centers of the

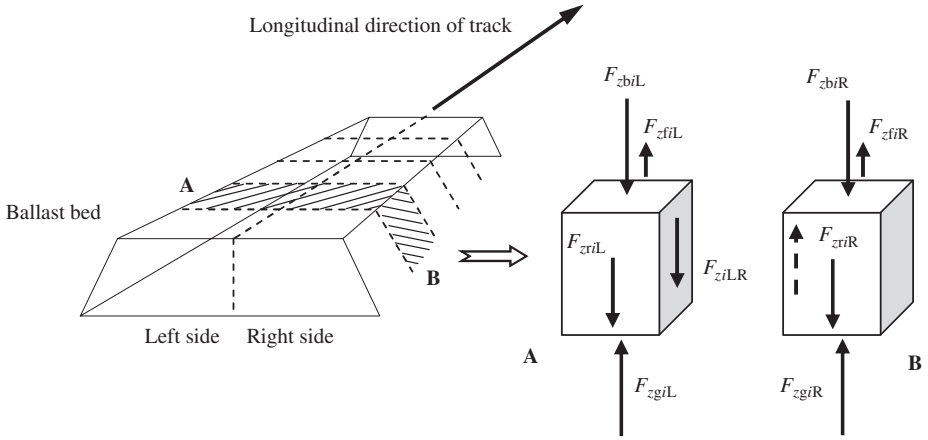

Fig. 7. Simplified calculation model of ballast.

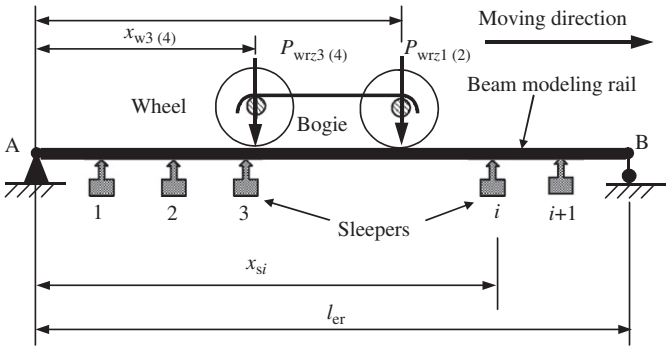

Fig. 8. Calculation model of wheels and rails.

ballast bodies is taken into account. In the model, it is obvious that the deformation of the ballast bed is not continuous during the vehicle passing. Probably the model cannot character the resonant frequencies and energy absorbing of the actual track exactly.

2.2.3. Model of wheel–rail contact

Due to neglecting the longitudinal accelerations of the system, the calculation model of the vertical (or lateral) interaction of the wheels and the rail (beam) is shown in Fig. 8. The half vehicle is statically placed at the center of a beam modeling the rail, the two ends of which are hinged. The coordinates $x_{wk}(k = 1, 2, 3, 4)$ indicate the position of the wheel k, with respect to the end A of the beam. They are constant in the calculation model. x_{si} is the coordinate of sleeper i. i ranges from 1 to 59. The length of the beam $l_{er} = 36$ m. Therefore, the second-order equations of the rails include the concentred forces by the sleepers and the wheels [35,36].

In the analysis of the transient coupling dynamics of the vehicle and the curved track, it is necessary that an accurate and quick calculation model of the coupling wheel–rail system is used. The calculation model of wheel–rail coupling usually includes the normal and tangential contact problems. Considering the influence of the wear of the rail running surface on the normal load, the usual model of the wheel–rail normal load reads

$$P_{\mathrm{wrn}k}(t) = \begin{cases} C_{\mathrm{H}}[Z_{\mathrm{wn}k} - Z_{\mathrm{rn}k} + \delta_0 - U_{\mathrm{w}k}]^{3/2}, & Z_{\mathrm{wn}k} - Z_{\mathrm{rn}k} + \delta_0 - U_{\mathrm{w}k} > 0 \\ 0, & Z_{\mathrm{wn}k} - Z_{\mathrm{rn}k} + \delta_0 - U_{\mathrm{w}k} \leqslant 0 \end{cases} \quad (1)$$

where $k = 1$, 2, 3 and 4 indicate wheels 1, 2, 3 and 4, respectively, $Z_{\mathrm{wn}k}$ and $Z_{\mathrm{rn}k}$ are the normal displacements of wheel k and the rail at their contact point, and they are determined by solving the system equations and calculating the contact geometry of the wheelset and the track (discussed later). δ_0 is the approach between the wheel and rail caused by the static normal load when the vehicle is on the central line of the track. $U_{\mathrm{w}k}$ is the depth of the accumulated wear on the rail running surface, at the contact point of wheel j and the rail. It should be noted that the model of the normal contact load Eq. (1) is approximately described with a Hertzian contact spring with a unilateral restraint. In Eq. (1), $Z_{\mathrm{wn}k} - Z_{\mathrm{rn}k} + \delta_0 - U_{\mathrm{w}k} > 0$ indicates the wheel–rail in contact, and $Z_{\mathrm{wn}k} - Z_{\mathrm{rn}k} + \delta_0 - U_{\mathrm{w}k} < 0$ stands for separation. C_{H} is the coefficient of the normal contact stiffness related to the Hertzian contact condition of the wheel and rail, selected as 1.13×10^{11} N/m$^{3/2}$ [38].

Shen–Hedrick–Elkins' model is adopted as the calculation model of the tangential forces between the wheels and rails [20]. The components, $F_{\tau xk}$ and $F_{\tau yk}$, of the instantaneous tangential force, and spin moment $M_{\mathrm{wrn}k}$ are easily and quickly calculated using the model of Shen et al. and with the known instantaneous normal load and the known instantaneous creepages. $F_{\tau xk}$ and $F_{\tau yk}$ denote the tangential force components in the longitudinal and lateral directions, respectively. $F_{\mathrm{wrz}k}$ and $F_{\mathrm{wry}k}$ are assumed to be the force components between the wheels and the rails, in the vertical and lateral direction respectively, and $M_{\mathrm{wrz}k}$ and $M_{\mathrm{wry}k}$ are the corresponding moment components. If $P_{\mathrm{wrn}k}$, $F_{\tau yk}$ and $M_{\mathrm{wrn}k}$ are obtained at any time instant, $F_{\mathrm{wrz}k}$, $F_{\mathrm{wry}k}$, $M_{\mathrm{wrz}k}$ and $M_{\mathrm{wry}k}$ are expressed in terms of $P_{\mathrm{wrn}k}$, $F_{\tau yk}$ and $M_{\mathrm{wrn}k}$, according to Fig. 9. They read

$$\begin{cases} P_{\mathrm{wrz}k} = P_{\mathrm{wrn}k}\cos\delta_k + F_{\tau yk}\sin\delta_k \\ F_{\mathrm{wry}k} = -P_{\mathrm{wrn}k}\sin\delta_k + F_{\tau yk}\cos\delta_k \\ M_{\mathrm{wrz}k} = M_{\mathrm{wrn}k}\cos\delta_k \\ M_{\mathrm{wry}k} = -M_{\mathrm{wrn}k}\sin\delta_k \end{cases} \quad (2)$$

In Fig. 9, vectors $\mathbf{n}$ and $\boldsymbol{\tau}$ denote, respectively, the normal and tangential directions of the wheel and the rail at their contact point. δ_k indicates the contact angle of wheel k and the rail. They are obtained through the contact geometry calculation of the wheelset and the track.

2.2.4. Initial and boundary conditions of track system

For the two-hinged ends of the Euler beam modeling the rails, the deflections and the bending moments at the beam ends should be zero. The deflection of the road bed is neglected; only the vertical deflections of the equivalent ballast bodies are taken

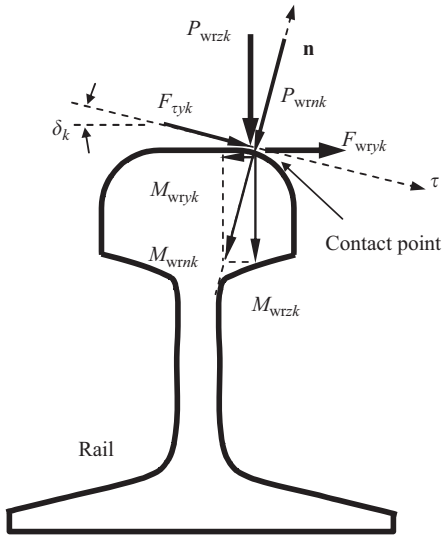

Fig. 9. Forces at contact point of rail.

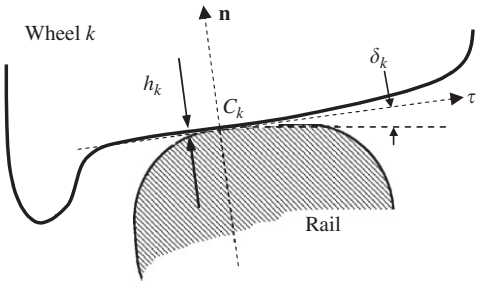

Fig. 10. Wheel k and rail in contact.

into account. The boundary conditions of the equivalent ballast bodies read

$$\begin{cases} Z_{bL0} = \dot{Z}_{bL0} = 0, & Z_{bL59} = \dot{Z}_{bL59} = 0 \\ Z_{bR0} = \dot{Z}_{bR0} = 0, & Z_{bR59} = \dot{Z}_{bR59} = 0 \end{cases} \quad (3)$$

Eq. (3) indicates that the vertical deflections and velocities of the equivalent ballast bodies next to the two ends of the track considered are zero.

Since the present system contains many differential equations and the detailed derivation of the equations is very tedious, the equations and their detailed derivation were omitted in the present paper. Zhai [38,39] developed a numerical method specifically to solve the coupled dynamic equations of the railway vehicle and track. The stability, calculation speed and accuracy of the numerical method for solving the equations were also discussed in detail.

2.2.5. Calculation model of wheel–rail contact geometry

In the rolling contact calculation of the wheels over the rails using non-Hertzian rolling contact theory by Kalker, the normal distances and the contact angles of the wheels and the rails, h_k and δ_k, as shown in Fig. 2, and also illustrated in Fig. 10, have to be previously calculated. In Fig. 10, C_k is the contact point of the rail and wheel $k(k = 1, 2, 3, 4)$, **n** and **τ** indicate, respectively, the normal and tangential directions at point C_k. The contact geometry parameters depend on Y_{wi}, ψ_{wi} and Y_{rk} for the prescribed sizes of the wheelset and the track. Y_{wi}, ψ_{wi} and Y_{rk} are obtained through the dynamics calculation of the vehicle curving.

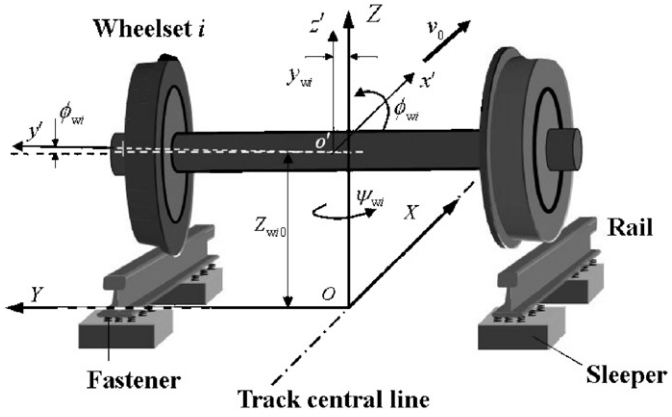

Fig. 11. Calculation model of contact geometry parameters of wheelset i and rails.

In order to find more accurate values of the contact geometry parameters, the method for the wheel–rail contact geometry analysis, discussed in Ref. [32], is further improved. Namely, according to the known instant Y_{wi}, ψ_{wi} and Y_{rk}, and the positions of the two rails in a fixed reference configuration $OXYZ$, as shown in Fig. 11, the height Z_{wi0} of the wheelset, in $OXYZ$, is set enough high to ensure no penetration occurred between the wheelset and the rails. The roll angle ϕ_{wi} of the wheelset, as shown in Fig. 11, is continuously changed in very small step size until the smallest distance between the left wheel and rail equals that of the right-side wheel and rail. Hence, for each side wheel and rail, there are two points with the smallest distance between them. One point is on the wheel tread, and the other is on the rail top. The two points constitute a pair of contacting points of the wheel and the rail before their deformations. At the known contact points, h_k and δ_k are determined based on the given profiles and the geometry sizes of the wheelset and the track. The profiles of the wheel and rail are expressed with the discrete datum, which are described in coordinate systems $OXYZ$ and $o'x'y'z'$, respectively, as shown in Fig. 11. The origin of $o'x'y'z'$ is fixed at the center of the wheelset, and its y'-axis coincides with the axle of the wheelset. Only the values of h_k in the analyzed square area covering the potential contact areas, seen in Fig. 12b, are calculated [31].

2.3. Rolling contact theory of wheel and rail

The normal pressure and the creepages between the wheel and rail determine contact stresses, stick/slip areas, frictional work density and wear volume in the contact area of the wheel/rail. They are related to the material service and mechanical behavior of the rail. Therefore, the two models, rolling contact mechanics and material wear, are simultaneously considered in the numerical simulation of rail wear and contact stresses. Until now Kalker's rolling contact theory of three-dimensional elastic bodies is very desirable in the rolling contact analysis of wheel and rail system in elastic region [30]. But, Kalker's theory needs to be modified little in the analysis. The modification is briefly explained in the following text.

In the complementary principle for three-dimensional elastic bodies in rolling contact, which is derived by Kalker, the virtual stress work in the contact area in the normal direction is written as (see at pages 10, 145 and 181 of Ref. [30])

$$e_J \delta p_{J3} = (A_{IiJ3} p_{Ii} + h_J - q)\delta p_{J3} \quad (4)$$

In Eq. (4) the repeated subscripts are summarized over their ranges. Subscripts $i = 1, 2, 3$ stand for the directions of x_1, x_2 and x_3 axes, respectively (see Fig. 12), I, J are the numbers of rectangular elements in Fig. 12b, p_{J3} is the component of the traction on

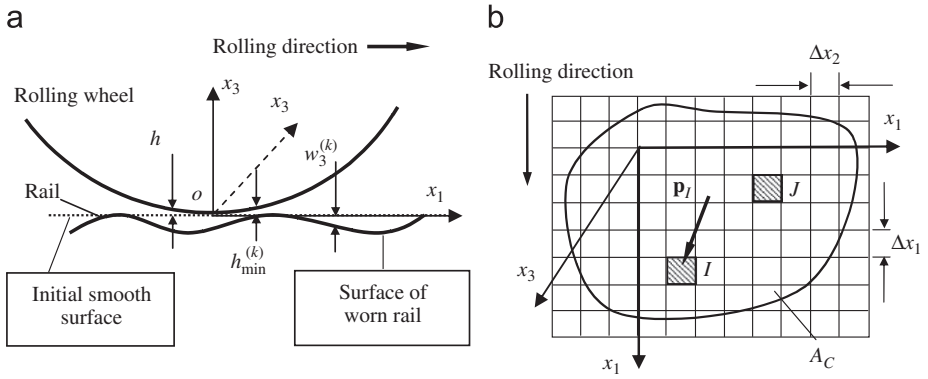

Fig. 12. (a) Description of normal distance variation and (b) uniform mesh covering a potential contact area.

rectangular element J in the direction axis x_3 (normal direction), δp_{J3} is its variation, p_{Ii} is the component of traction on element I in the i-direction, A_{iIJ3} is the influence coefficient of force/displacement, indicating the x_3-direction displacement occurring at the center of rectangular element J caused by the i-direction unit force at the center of rectangular element I, q is the unknown approach of the wheel and rail in the direction of x_3. h_J is the value of h at the center of rectangular element J. When considering the influence of wear depth $w_3^{(k)}$, after k passages of the wheel rolling, on the normal stress virtual work, we need to modify Eq. (4) to calculate the virtual stress work in discrete form. Eq. (4) is changed to

$$e_J^{(k)}\delta p_{J3} = [A_{IiJ3}p_{Ii} + (h_J + w_{3J}^{(k)} - h_{\min}^{k}) - q]\delta p_{J3} \tag{5}$$

where $h_{\min}^{(k)}$ is the minimum of the normal gap between the wheel and rail, shown in Fig. 12a. So, we write the discrete form of the principle of complementary virtual work of the wheel and rail in rolling contact as follows:

$$\begin{cases} \min C = \frac{1}{2}p_{Ii}A_{IiJj}p_{Jj} + [(h_J + w_{3J}^{(k)} - h_{\min}^{k}) - q]p_{J3} + (W_{J\tau} - u'_{J\tau})p_{J\tau} \\ s.t.: p_{J3} \geqslant 0,\ |p_{J\tau}| \leqslant b_J, \\ A_0 \sum_{J=1}^{M} p_{J3} = P,\ \forall x \in A_c \end{cases} \tag{6}$$

In Eq. (6) subscripts $\tau = 1, 2$ denote the directions of x_1 and x_2, A_{IiJj} are the influence coefficients of force/displacement, indicating the occurrence of the i-direction displacement at the center of rectangular element I caused by the j-direction unit force at the center of rectangular element J. A_{IiJj} is easily obtained based on the theory of elastic half space [30]. $u'_{J\tau}$ is the component of the elastic displacement difference of the pair of contact particles at the center of element J, at the previous time step t'. The rectangular element area is equal to $A_0 = \Delta x_1 \times \Delta x_2 = 0.8 \times 0.8 = 0.64\,\text{mm}^2$, A_c is the potential contact area, M is the total number of elements, selected as $21 \times 21 = 441$ in the calculation. b_J is the bound of Coulomb friction at the center of element J, which reads

$$\left.\begin{aligned} b_J &= fp_{J3} \quad x \in H \\ b_J &= f' p_{J3} \quad x \in S \end{aligned}\right\} \tag{7}$$

where f, f' are, respectively, the static and kinetic friction coefficients of Coulomb. The friction coefficient between the wheel and rail depends on many factors, such as the status of the contact surfaces of the wheel and rail, the material, the geometry size, the environment, etc. So far it cannot be expressed with a complete mathematical form. Usually it is selected as a constant in range from 0.3 to 0.5 in the numerical simulation of railway vehicle and track dynamics. Therefore, we select $f = f' = 0.3$ in the calculation. H and S are, respectively, the stick area and slip area in the contact area. In Eq. (6), P is the total normal load. For the contacts of the wheels and rails shown in Fig. 4b, $P = P_{\text{wrn1}}$, P_{wrn2} P_{wrn3} and P_{wrn4}, defined by Eq. (1). $W_{J\tau}(\tau = 1, 2)$ is the component of the rigid slip between the wheel and rail at the center of element J from the previous time step t' to the present time step t, and written as

$$W_{J\tau} = \int_{t'}^{t} [\xi_{\tau k} + (-1)^{\tau} x_{3-\tau}\xi_{3k}]v_0 \mathrm{d}\varsigma \quad \tau = 1, 2, \quad k = 1, 2, 3, 4 \tag{8}$$

In Eq. (8), $\xi_{\tau k}(k = 1, 2, 3, 4)$ denotes the creepages of wheel k respectively, and obtained through the dynamics analysis discussed above. The Mathematical Programming Method is used to find the solution to Eq. (6) [30]. The components of the traction, p_{Ji} $(i = 1, 2, 3)$, are obtained. $W_{J\tau}$ and p_{Ji} are used in the calculation of the frictional density. It should be stated that Kalker developed a computer code CONTACT to carry out the numerical calculation of three-dimensional elastic bodies in rolling contact with non Hertzian form. The code is modified and used in the present calculation. The modification reflects that, for each calculation step of the wheel rolling in Δx_1, h_J and $w_J^{(k)}$ need to be updated. Namely, the effect of the wear caused by the previous calculation step is taken into account in the present step, as shown in Fig. 13. Also the modified code can be used to simulate the continuous and repeated rolling of the wheel over the rail. Through such numerical simulation of the continuous and repeated rolling of the wheel, the accumulated rail wear and contact stresses at any instant step are found.

2.4. Material wear model of rail

The material wear model in which material loss mass of unit area is proportional to frictional work of unit area reads [32,33]

$$\Delta m(x_{I1}, x_{I2}) = C_w f_w(x_{I1}, x_{I2}) \tag{9}$$

In Eq. (9), (x_{I1}, x_{I2}) are the coordinates of the center of element I, the $\Delta m(x_{I1}, x_{I2})$ and $f_w(x_{I1}, x_{I2})$ are, respectively, the material mass loss of unit area and the friction work density at point (x_{I1}, x_{I2}), the proportional coefficient $C_w = 1.0 \times 10^{-9}\,\text{kg}\cdot(\text{N m})^{-1}$ [40]. Considering $S_{I\tau}$ and p_{Ij} as constants in square element I, Eq. (9) is rewritten as

$$\Delta m(x_{I1}, x_{I2}) = C_w f_w(x_{I1}, x_{I2}) = C_w |S_{I1}p_{I1} + S_{I2}p_{I2}| \tag{10}$$

The component of the total slip at the center of element J from the previous time step t' to the present time step t, $S_{J\tau}$ reads

$$S_{I\tau} = W_{I\tau} + p_{J\tau'}A_{J\tau' I\tau} - u'_{I\tau}\ (\tau, \tau' = 1, 2,\ I, J = 1, 2, \ldots M) \tag{11}$$

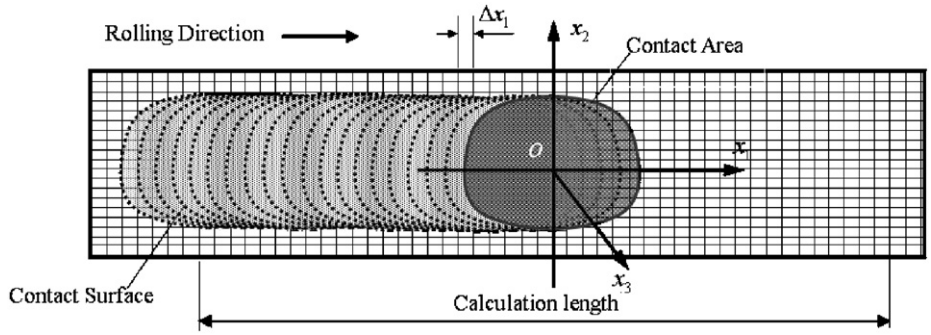

Fig. 13. Rail running surface passed by contact area.

After a first passage of the wheel, the depth of wear at the center of element I, on the running surface of rail, is written as

$$w_{I3}^{(1)} = C_w|S_{I1}p_{I1} + S_{I2}p_{I2}|/\rho \tag{12}$$

where $\rho = 7.8 \times 10^3\,\mathrm{kg\,m^{-3}}$, which is the density of the rail material. After k passages the total wear depth is the sum of each wear depth.

Using the above procedure, the wear volume and contact stresses occurred on the rail running surfaces passed by the 4 wheels of the same bogie are predicted when the half vehicle curving the prescribed track.

2.5. Discussions on similar existing models

The present model considers the combination of the model of vehicle and track interaction, the model of wheel and rail in rolling contact, and the model of rail material loss. It describes the feedback loop process between the transient curving dynamics of vehicle and track and the rail profile change due to wear. The model of vehicle and track interaction is a three-dimensional one in time domain. The present model has some disadvantages and needs to be further improved.

It should be noted that, for the introduced rail material wear model, the effect of material working-hardening, due to repeat rolling and press of wheels, on the wear is neglected. Furthermore, the profile change of the rails in service, due to the plastic deformation caused by loaded wheel passing, cannot be taken into consideration in the present model since up to now no mathematical model can simultaneously represent the wear and plastic deformation of rail material, and their interaction in the increasing of wear and plastic deformation, as shown in Fig. 1b. Fig. 1b shows severe corrugation occurring on a curved track due to combination of accumulated wear and plastic deformation. The profile of the passing wheels is assumed to be invariable, namely, the profile change of the wheels, due to wear and plastic deformation, is neglected, as indicated by Fig. 12a. If the present model is going to be used to analyze the dynamical behavior of wheel and rail in rolling contact at high frequencies at high speeds, it should consider the flexible wheelsets and the nonlinear physical properties of the track parts, such as rail fastening system, ballast, etc. Usually, the dynamic behavior at high frequencies mainly includes noise, rail short pitch corrugation related to noise and vibration, and possibly growing of cracks on wheel and rail.

In the modeling for vehicle and track interaction, the half vehicle is placed at the center of the track with a selected finite length, and always in static state with the track, as indicated by Fig. 8. Such a track model in the present analysis cannot represent the effect of discrete sleeper supporters moving with respect to the running vehicle on the dynamical behavior. The present model is not available for investigation into the short pitch corrugation on tangent track. Such a short wavelength wear on rail is possibly related to the rail discrete sleepers and the high speed of vehicle. Published papers [35,36] used the same model as the present paper. In order to analyze the effect of rail irregularity on the dynamic behavior of vehicle and track interaction, an assumed strip containing such irregularities on the railhead was effectively pulled at a steady speed between wheel and rail [35,41]. However, such an irregularity strip cannot model the effect of the motion of the discrete sleeper supporters, with respect to the running vehicle exactly. When the analysis on the vehicle curving at a constant speed was carried out with the present model in these papers, the inertia forces of the vehicle parts related to the constant curving speed were considered in the differential equations of the parts [35,36]. So, the present model can consider the effect of the curving speed on the dynamic behavior of the vehicle passing through the curved track with smooth rails. But at a tangent track with smooth rails, the model can not be used to investigate the effect of the speed since the inertial forces of the vehicle parts caused by the curving disappear in the motion equations, except for the irregularity strip introduced. In addition, an Euler beam model replacing the rails in the track model is not exactly available for characterizing the dynamic behavior at high frequencies larger than 800 Hz since the effect of rotation inertia and shear deformation in Euler beam theory is ignored [42]. Ref. [42] made a detailed investigation into the difference between the vertical resonant frequencies characterized by the models of Euler and Timoshenko beams. The results in [42] were compared to the experiment results by Grassie [43]. It was found that the result by Timoshenko beam is in good agreement with the experiment result. The model in [42] is only available for investigation into track natural vibration characteristics in frequency domain in vertical direction, and track response under a vertical stationary impact load. The vehicle model is simple. It is well known that using the finite element model for rail will obtain the more accurate results than Timoshenko or Euler beam. But the finite element method is the most time-consuming, and is difficultly used directly in the fast three-dimensional numerical simulation of vehicle and track interaction in time domain so far because of existing unadvanced numerical methods and insufficient capability of computers. It is not difficult to use Timoshenko beam to model rail in modeling of track in time domain. The work is almost accomplished by the group of the present authors. With the track model considering Timoshenko beam replacing rails, some numerical results regarding derailment and other dynamic behaviors will be published. In the investigation into track noise, track model needs to consider not only the resonant frequencies of flexible wheel/rail, but also the resonance frequencies of flexible sleepers because the sleeper is one of track noise sources that generate noise with vibration frequencies up to 1000 Hz [44]. Hence, the sleeper should be modeled by finite element method

or Timoshenko beam with variable cross section. This work is under way.

In the modeling for track components, it is the most difficult to model track ballast due to the ballast deflecting in a highly nonlinear manner under load. The dynamic load transmitted through the ballast causes friction, compress and separation in ballast aggregate that is a congeries of break-stones with irregularity boundaries and inhomogeneous physical properties. So its dynamic behavior is still an area of ignorance [37]. Zhai et al. [38,39] used additional ballast masses below each sleeper which are interconnected by springs and dashpots in vertical shear. Such a ballast model was firstly put forward by Sato in 1987 [37], and is used in the present modeling for track, as shown in Fig. 4. However, the five parameters of the ballast model (stiffness and damping values for the shear connection and for the substrate, plus the ballast mass) may make it difficult to obtain satisfactory parameter values from experimental data. Zhai [36] has accordingly tried to estimate the five parameters theoretically. If the satisfactory values of the five parameters can be obtained, the more equivalent ballast bodies under each sleeper can be used to represent the ballast dynamic behavior, as shown in Fig. 14. This ballast model indicated by Fig. 14 can characterize the vertical dynamic behavior of the ballast better than that in Fig. 4. In Fig. 14, F_{zLi} and F_{zRi} are the vertical forces between rails and sleeper, subscripts L and R indicate, respectively, the left and right. k_{beq} and c_{beq} denote, respectively, the stiffness and damping coefficients per unit lateral length, under a sleeper. Fig. 14 shows that this track model considers flexible sleepers, and ignores the motion of the subgrade. The numerical implementation of Fig. 14 is being under way. If the ground-borne vibration caused by a passing train at high speed is of interest, the subgrade indicated by Fig. 14 should be considered and represented by finite element model or boundary element model.

These important factors discussed above will be gradually taken into consideration in the modeling for vehicle and track interaction at high frequencies and high speed.

Similar to the model described by Fig. 2, another model regarding feedback loop concept was used to predict rail head wear caused by a wheel rolling over short-wavelength longitudinal irregularities on the rail in time domain by Igeland and Ilias [40]. In their model, the vehicle was treated as a single wheel connected via primary springs and dampers to a rigid body. Infinite Timoshenko beam was used to model rail (this track model developed by TU Berlin). The sleeper was considered as a rigid body. The ballast mass and the subgrade motion were not taken into consideration. The models for wheel and rail in rolling contact and rail material wear are the same as those in present study. But their model is restricted to vertical dynamics only. The lateral friction force, the spin moment, and the lateral and the spin creepages were assumed to be zero. The numerical results showed the growth of short-wavelength longitudinal irregularities on the rail with increasing wheel passes.

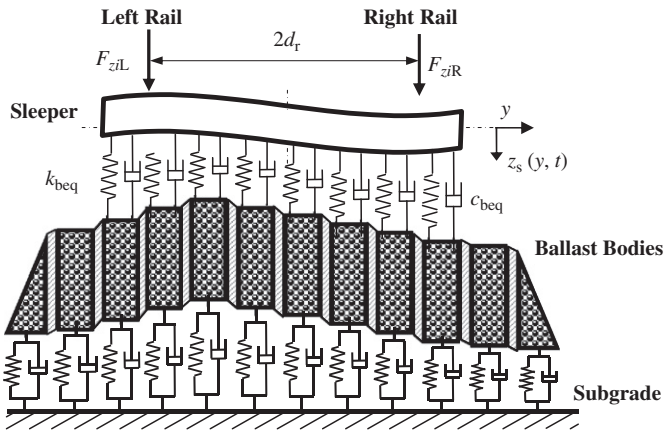

Fig. 14. Ballast model in vertical direction.

In the analysis on the wear of wheel and rail in rolling contact, the most of results published were obtained through experiments with small-scaled test facilities [9–17]. Although these obtained results are very important and very useful in understanding the material wear mechanism of wheel and rail and their behavior improvement, they are not completely consistent with wear phenomena occurred on wheel tread and rail top since small-scaled facilities can not completely reproduced the service circumstances of the wheel and rail. To date no results on the wear of wheel and rail through experiments with full-scaled facilities were reported. The findings in [10,11,17] promote the present numerical simulation on the wear of wheel and rail. However, it seems that the wear rate of wheel and rail material described by the wear model in the present study is faster than that in practice. Paper [19] used the total frictional work in the contact patch of wheel and rail to evaluate the influence of curved rail lubrication on the rail material wear. The thinking of Shen et al. is concerned with the wear volume proportional to the frictional work. Jendel [21] developed a tool for prediction of wheel wear with help of Archard's wear model. The advantage of Archard's wear model is that it considers material hardness. But the material hardness of wheel and rail varies with the passes and loads of wheel. So far it seems to be difficult to represent the variation of the hardness with mathematical expression. If the problem cannot be solved completely, it is impossible to accurately predict the wear of wheel and rail. Jendel used a constant hardness of wheel material in his calculation. In addition, wear still occurs without a slip between wheel and rail when the material of the wheel and rail exceeds ductility limit. Small debris generate under large shear force between the contacting surfaces of wheel and rail, since the subsurface material of the wheel and the rail exceeds the ductility limit and the small subsurface cracks form and propagate parallel to the contact surface, and finally intersect. Such a wear phenomenon can not be so far described with mathematical expressions. Hence, it is very difficult to carry out the numerical simulation on wheel and rail wear due to the accumulated material plastic deformation exceeding the material ductility limit.

In the calculation of contact stresses and material wear of wheel and rail in rolling contact, it is very desirable to use Kalker's theory of three-dimensional elastic bodies in rolling contact [30,35,36]. The assumptions used in Hertzian contact theory will be broken in the circumstances of the great change of wheel and rail profiles or the irregularities with wavelength less than the typical diameter of the contact patch. After long time use of wheel and rail, the curvature radii of the wheel and rail profiles in the lateral and longitudinal directions vary due to wear. They are not constants at and around the contact point. Which values of them are available for the calculation of the some parameters in Hertz contact theory? However, when using Kalker's theory with non Hertzian form calculates the contact stresses and the material wear of the worn wheel and rail, regardless of the variation of the curvature radii, it needs only the normal distance (gap) between the worn wheel and rail at and around the contact point, which is calculated by using the geometry boundaries of the worn wheel and rail at or around the contact point. It is satisfactory to calculate the contact stresses and the material loss distributed on the rail top [35,36] with Kalker's theory. But the application of Kalker's theory is still restricted due to elastic half-space assumption used in the numerical implementation of the theory. Probably using finite element method achieves the more accurate

results on rolling contact [45]. But the progress in this area is very slow.

3. Numerical example and discussions

In the numerical analysis, a great number of the structural parameters are used. Their selection was shown in Refs. [35,36,38]. The rail wear location is selected at about the center of the circle curve, as shown in Fig. 15. In Fig. 15 point *O* is the center of the circle curved track. The *Y*-axis points to the right side of the track, *X*-axis the forward direction of the vehicle. Through the dynamics analysis, we obtain the displacements, velocities, accelerations, spring and damper forces of the system, the creep forces, creepages and material weal volume of the wheels and rails. Some of the interesting results are shown in the following text, and discussed in detail.

3.1. Effect of curving speed

In this case, the super-elevation h_t is 100 mm, the rail cant α_t is 1/40, and the curving peed v is selected as 80, 100 and 120 km/h, respectively. When the half vehicle passes the center of the circle curved track at 80, 100 and 120 km/h, respectively, as shown in Fig. 15, the variations of the parameters, concerning the behavior of the wheelset and track, are listed in Table 1. In the table, Numbers 1, 2, 3 and 4 indicate, respectively, wheels 1, 2, 3 and 4. ① and ② stand for the leading and trailing wheelsets respectively. Sign "-" indicates the corresponding variable in the opposite direction with respect to *X*- or *Y*-axis. The unit of the wear volume "mm^3/mm" indicates 1 mm^3 material loss per 1 mm along the rail running surface.

From Table 1, the difference between the normal loads of the left and right wheels/rails increases much with increasing the curving speed. The normal load difference between the left and right wheels of the leading wheelset increases by 37%, and that for the tailing wheelset increases by 51%. This is mainly caused by the increasing of the centrifugal force of the vehicle due to the curving speed increasing. When the speed increases from 80 to 120 km/h, the total lateral creep force of the leading wheelset increases from −14.3 to 4.3 kN. The lateral force is caused by the curved track, and in the opposite direction of *Y*-axis, namely, points to the outside of the track. The longitudinal creep force on the wheel 1(left wheel) is in the direction of *X*-axis, and that of wheel 2 in the opposite direction of *X*-axis. The pair of the longitudinal creep forces on the left and right wheels of the leading wheelset makes the effect that is propitious to the curving of the wheelset. It is obvious that the attack angle of the leading wheelset against the curved track decreases from 0.085° to 0.028° when the curving speed ranges from 80 to 120 km/h. According the results, it is found that the leading wheelset has a good curving performance under the present conditions, which include the prescribed curving speeds and the prescribed geometry sizes of the wheelset and track. The situation regarding the longitudinal creep forces on the trailing wheelset is reverse. Namely, the effect of the longitudinal creep forces on the trailing wheelset is not good for the trailing wheelset curving. But the longitudinal creep forces of the trailing wheelset are very small, and decrease with increasing the speed. The yaw angle (attack angle) of the trailing wheelset is very small, but increases with the speed increasing. The negative lateral displacements of the centers of the wheelsets increase with increasing the curving speed. Namely, the increasing curving speed makes the wheelsets approach to the outside rail (high rail) of the curved track. In the present situation, no flanging action of the outside wheel/rail occurs due to the large radius of the curved track. The lateral displacement of the leading wheelset is larger than that of the trailing wheelset at the speeds of 80, 100 and 120 km/h.

The rail wear caused by the wheels 1, 3 (outside wheels) decreases with the speed increasing from 80 to 100 km/h, and increases from 100 to 120 km/h. The wear caused by wheels 2 and 4 grows with increasing the speed. For the cases of the three

Table 1
Effect of curving speed on behavior of wheels/rails in rolling contact

$\alpha_t = 1/40$, $h_t = 100$ (mm)	Wheels	$v = 80$ km/h	$v = 100$ km/h	$v = 120$ km/h
Normal load (kN)	**1**	**55.2**	**60.4**	**66.8**
	2	57.2	52.0	45.8
	3	56.9	63.4	70.7
	4	54.9	49.0	41.9
Lateral creep force (kN)	1	−5.7	−4.7	−2.6
	2	−8.6	−4.9	−1.7
	3	9.6	7.1	13.3
	4	3.2	6.1	8.9
Longitudinal creep force (kN)	1	15.5	16.6	19.2
	2	−13.9	−14.7	−13.6
	3	−2.7	−2.0	0.6
	4	3.1	2.3	−0.79
Maximum normal pressure (MP_a)	**1**	**882.2**	**1459.1**	**994.9**
	2	710.2	710.2	645.9
	3	1028.8	1028.9	718.1
	4	1017.4	1017.4	716.4
Maximum lateral creep force density (MP_a)	1	105.9	132.6	65.5
	2	120.3	59.4	34.3
	3	259.6	197.2	199.2
	4	126.4	218.1	203.0
Maximum longitudinal creep force density (MP_a)	**1**	**242.5**	**417.2**	**297.1**
	2	176.0	148.0	190.7
	3	76.5	50.0	19.9
	4	123.7	90.2	17.2
Wear volume (mm^3/mm)	1	0.00781	0.00688	0.00705
	2	0.00481	0.00502	0.00613
	3	0.00144	5.49E−4	0.00201
	4	1.72E−4	5.09E−4	0.00136
Wheelset center lateral displacement (mm)	①	−6.650	−7.024	−8.052
	②	0.080	−4.027	−6.243
Wheelset attack angle (deg.)	①	0.085	0.058	0.028
	②	−0.020	−0.048	−0.087

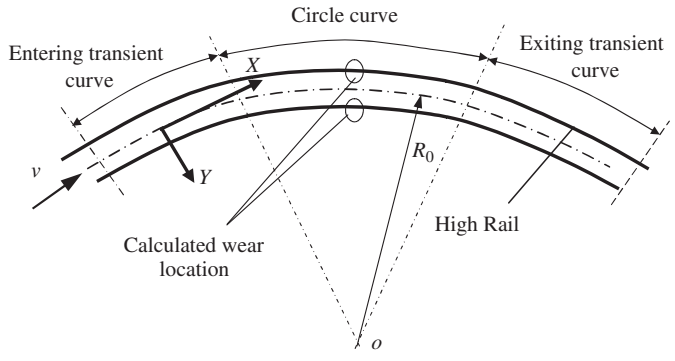

Fig. 15. Location of rail wear analyzed on the curved track.

different speeds, the rail wear volume caused by wheel 1 is the largest. Usually, the wear caused by the wheels keeps growth with further increasing the speed. But, the increasing of the curving speed is limited by the super-elevation of the curve track. Otherwise, the difference between the normal loads on the left and right wheels of the same wheelset further increases, as listed in Table 1. The difference between the use life of the left and right rails increases. The use life of the high rail of the curved track becomes much shorter than that of the low rail. The left and right rails in service can not reach the same long use life. They can not be used as perfectly as possible. In addition, the too high curving speed can lead to the turnover of the vehicle to outside, and derailment accident occurs.

The maximums of the absolute values of the contact stresses between the 4 wheels and the rails are listed in Table 1. Compared them with the corresponding total forces between the wheels and the rails, their variations with the curving speed are different. Taking wheel 1 as an example, see the bold numbers shown in Table 1, the normal load of wheel 1 is 60.4 kN at 100 km/h, which is larger than that at 80 km/h, and less than that at 120 km/h. But the maximum of the normal pressure is much larger than those at 80 and 120 km/h. The normal pressures for the three speeds are illustrated by Fig. 16. Signs A, B and C indicate the cases of 80, 100 and 120 km/h, respectively. According to the friction law, the large normal pressure leads to the large tangent traction. Fig. 17 illustrates the distributions of the corresponding longitudinal creep forces. So, the contact stresses depend not only on the total forces, but also on the contact patch of the wheel and the rail. The corresponding patches for the three speeds are shown in Fig. 18. The total contact area, stick area and slip area of wheel 1 are, respectively, 94.4, 0.0 and 94.4 mm^2 at 80 km/h; 72.8, 11.2 and 61.6 mm^2 at 100 km/h; and 103.2, 9.6, and 93.6 mm^2 at 120 km/h. The contact area at 100 km/h is smaller than those at the speeds of 80 and 120 km/h. The contact area at 120 km/h is the largest. Hence, the maximum of the normal pressure at 100 km/h is much larger than those in the other two cases. The areas with arrows in Fig. 18 indicate the slip areas, and the empty areas stand for the stick areas in the contact patches. The stick areas exist in the contact patches at 100 and 120 km/h since the normal pressures increase and the total slips in the contact area of the wheel and rail decrease. The total slip includes the slip related to the creepages and the slip caused by the elastic deformation of the wheel and rail. The creepages are not shown in the present paper. Except for the normal load, the contact patch size and its shape depend on the profiles of the wheel/rail.

When the vehicle passes at 100 km/h through the center of the circle curved track, the lateral displacement and the yaw angle of

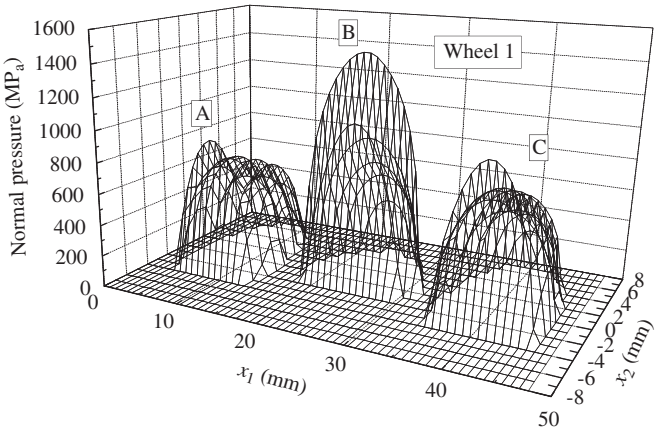

Fig. 16. Normal pressures of wheel 1 at 80, 100 and 120 km/h.

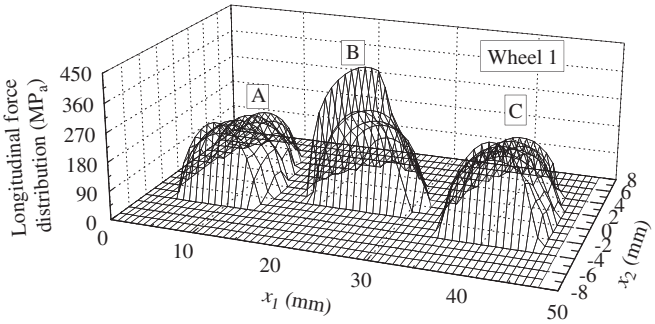

Fig. 17. Densities of longitudinal creep forces of wheel 1 at 80, 100 and 120 km/h.

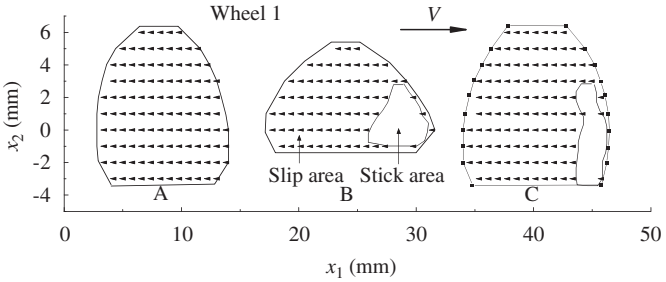

Fig. 18. Stick/slip areas of wheel 1 at 80, 100 and 120 km/h.

the leading wheelset are, respectively, −7.024 mm and 0.058°, where the profiles of the outside wheel/rail do not match very well. In order to decrease the normal pressure to extend the use life of wheel and rail in service, not only the normal load is decreased as low as possible but also the profiles are as conformable as possible. The normal load is concerned with the curving speed and the characters of the vehicle and track. The normal load is reduced by improving the characters of the vehicle and the track. The efficient decreasing of the normal pressure is to shorten the normal gap formed by the wheel/rail profiles. The normal gap is described with h_t, as shown in Fig. 10. The smaller normal distance leads to the larger contact area and the lower normal pressure under the condition of the constant normal load. On the other hand, the improvement of the profiles deteriorates the curving behavior of the vehicle probably. Therefore, both the profiles and the curving behavior are simultaneously considered to be improved in the design of the vehicle and the track. This is, however, a complicated project.

3.2. *Effect of super-elevation of curved track and rail cant*

In the improvement of the curving behavior of the vehicle, optimizing the sizes of the track is a good measure. In this section two cases are considered. The first case analyzes the effect of the super elevation h_t on the rail wear and the contact stresses under the condition that the curving speed $v = 120$ km/h, and the rail cant $\alpha_t = 1/40$. The super-elevation h_t is selected as 100, 120 and 140 mm, respectively. In the second case, $h_t = 120$ mm, $v = 120$ km/h and $\alpha_t = 1/40, 1/30$ and $1/20$. Figs. 19a, 20a and 21a illustrate the variations of the normal load, the maximum normal pressure and the wear volume, respectively, with increasing h_t. Figs. 19b, 20b and 21b indicate the variations of the corresponding parameters with increasing α_t. The difference between the normal loads of the left and right wheels of the wheelset decreases linearly with increasing h_t. Increasing h_t is beneficial to the safe curving of the vehicle and the equilibrium use of rail life in service. Increasing α_t leads to the increasing in the difference

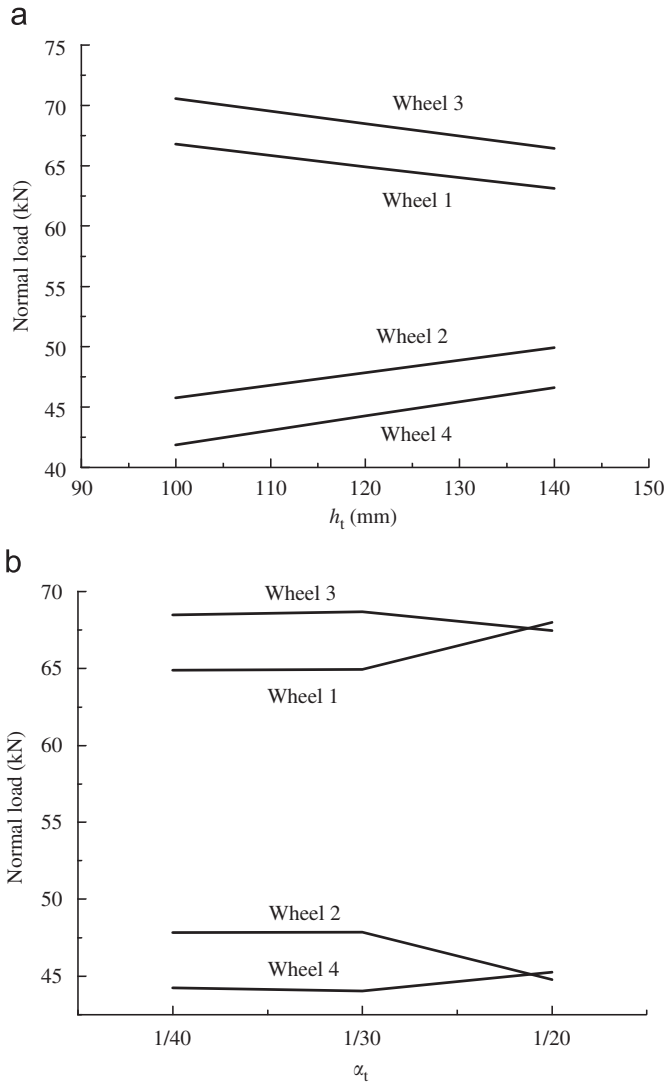

Fig. 19. (a) Normal load vs. h_t for $v = 100$ km/h and $\alpha_t = 1/40$, (b) normal load vs. α_t for $v = 120$ km/h and $h_t = 120$ mm.

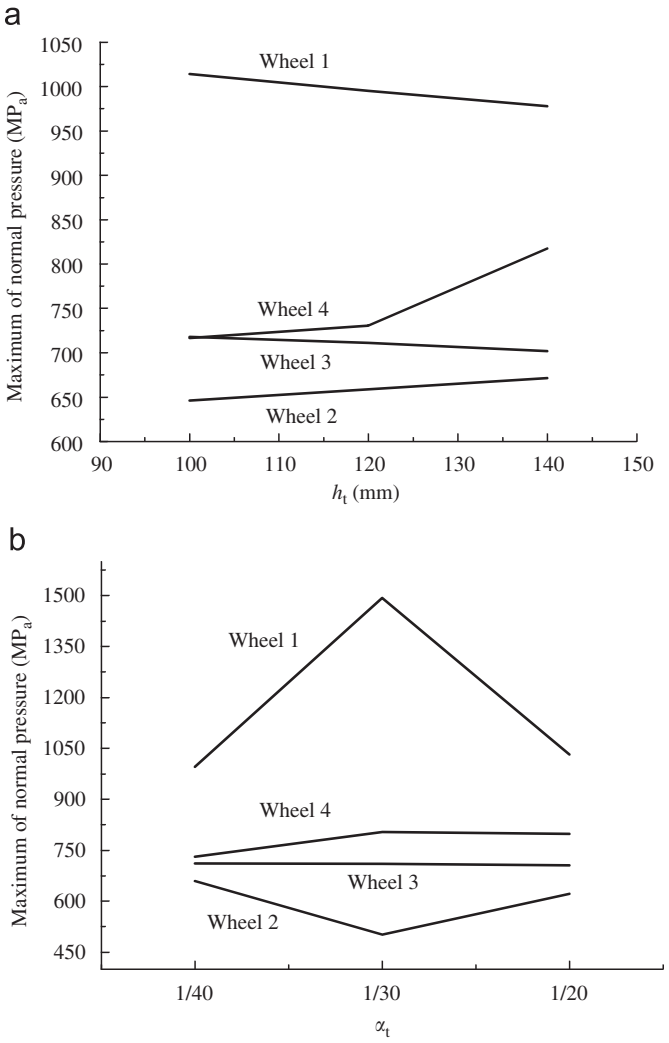

Fig. 20. (a) Normal pressure maximum vs. h_t for $v = 100$ km/h and $\alpha_t = 1/40$ and (b) normal pressure maximum vs. α_t for $v = 120$ km/h and $h_t = 120$ mm.

between the normal loads of wheel 1 and wheel 2, and the decreasing in that of wheel 3 and wheel 4, as shown in Fig. 19b. When α_t reaches $\frac{1}{20}$, the normal load of wheel 1 approaches to that of wheel 3, and the normal load of wheel 2 goes near that of wheel 4.

The maximum normal pressure of wheel 1 is always larger than those of the other three wheels, as shown in Fig. 20. The severest wear and rolling contact fatigue usually occur on the high rails of curved tracks at railway sites. The wheel 1 or the outside wheel of the leading wheelset dominates the rail damage. So, to lower the contact stresses is one of main objects in the improvement of the vehicle and the track. It is hoped that the larger contact stresses go down and the smaller ones go up for the 4 wheels of the same bogie through the improvement. Fig. 20a shows that the maximum normal stresses of wheel 1 and wheel 2 goes down and those of the other two wheels go up with increasing h_t. Their variations depend on the variations of the normal loads and the contact areas. The contact areas are omitted due to the paper size limited. For the second case, the level of the contact stresses at $\alpha_t = 1/40$ is almost the same as that at $\frac{1}{20}$, as shown in Fig. 20b. From the figure, $\alpha_t = 1/30$ is probably a bad choice. Based on the results of Figs. 19b and 20b and in consideration of the balance in selection of the good behavior and the low contact stresses, it is suggested that $\alpha_t = 1/20$ is selected as the best choice in the rail cant selection. If the results shown in Fig. 20 need to be improved further, the profiles of the wheel and the rail can be further improved. The work will be carried out in the near future.

The rail running wear is a kind of rail damage patterns. It also controls the use life of the rail in service. The severe wear changes rail profile much, and the curving behavior of the vehicle becomes bad. The inferior behavior of the vehicle may lead to the occurring of many bad things, such as the larger contact loads and stresses, the lower riding comfort, the serious hunting (unsteady), the derailment, etc. The larger loads and stresses break the rail easily and suddenly, which causes a derailment accident. Therefore, decreasing rail wear is an important measure to prolong the use life of the rail. Decreasing rail wear mainly relies on the reduction of the normal contact stress, the creepages, and the rail material hardening. The normal stress is discussed above. The effect of the rail material hardening on the wear does not belong to the work of the present paper. The creepages of the wheel/rail systems are related to the instant motion of the vehicle and the track, the profiles of the wheel and the rail, and the geometry sizes of the wheelset and the track. The present paper does not in detail

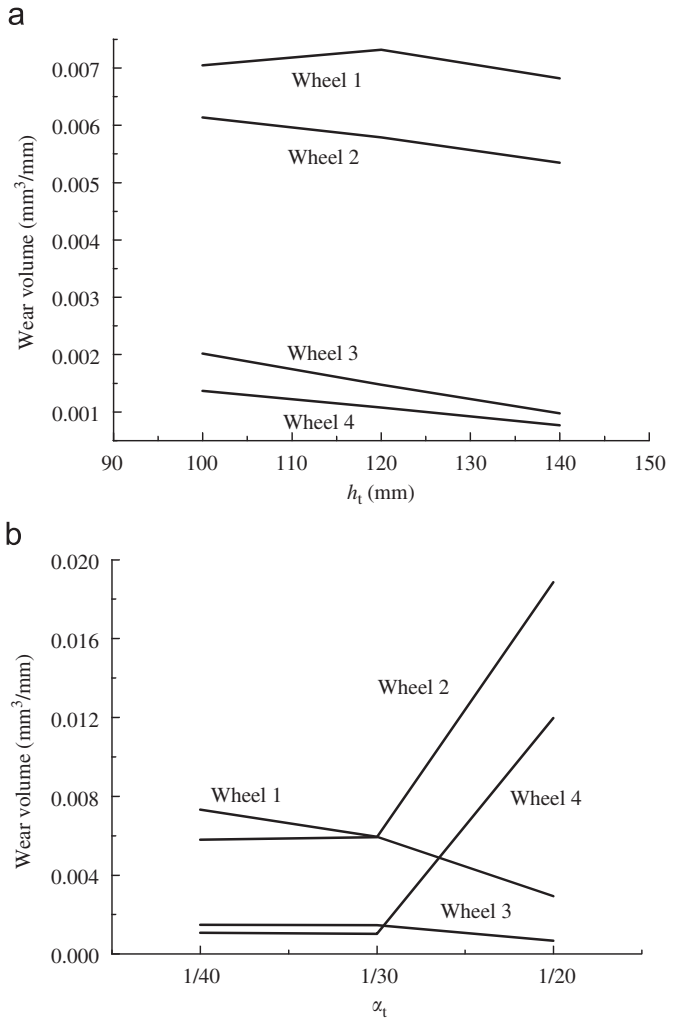

Fig. 21. (a) Wear volume vs. h_t for $v = 100$ km/h and $\alpha_t = 1/40$ and (b) wear volume vs. α_t for $v = 120$ km/h and $h_t = 120$ mm.

Table 2
Creepages, lateral displacements and yaw angle of wheels

$h_t = 120$ (mm), $v = 120$ km/h		$\alpha_t = 1/40$	$\alpha_t = 1/30$	$\alpha_t = 1/20$
Lateral creepage	1	5.74E−4	6.39E−4	0.00187
	2	6.04E−4	6.61E−4	0.00206
	3	−0.00129	−0.00128	−9.07E−4
	4	−0.0013	−0.00129	−9.38E−4
Longitudinal creepage	1	−0.00321	−0.00286	−6E−6
	2	0.00337	0.00342	0.01103
	3	7.3E−5	−1.9E−5	−1E−6
	4	−1.12E−4	2.8E−5	0.00709
Wheelset center lateral displacement (mm)	①	−8.09	−7.83	−7.65
	②	−6.28	−5.625	−5.66
Wheelset attack angle (deg.)	①	0.028	0.0374	0.0345
	②	−0.087	−0.0743	−0.0749

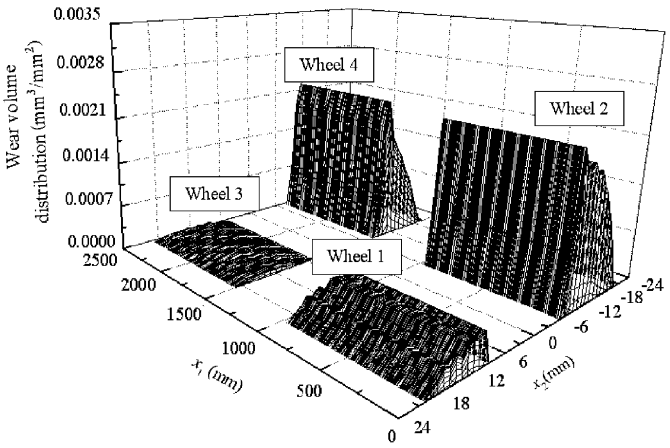

Fig. 22. Rail wear distribution on the tops of the rails.

discuss the effect of the change of the profiles on the wear. Fig. 21a and b illustrates the effects of the super elevation and the rail cant on the rail wear volume, respectively. For $v = 100$ km/h and $\alpha_t = 1/40$, the wear volumes caused by the 4 wheels decrease with increasing h_t. For $v = 120$ km/h and $h_t = 120$ mm, the wear volumes caused by wheels 1 and 3 decrease, and those by wheels 2 and 4 increase much with increasing α_t. But there is not much change in the normal load when α_t changes, as shown in Fig. 19b. Also the maximum normal pressure is not so high at $\alpha_t = 1/20$, as shown in Fig. 20b. Therefore, the severe wear caused by wheels 2 and 4 on the low rail running surface should be attributed to the much change of the creepages. When α_t increases from $\frac{1}{40}$ to $\frac{1}{20}$, the creepages of the wheels and the rails change very much. Their much change is caused by only a little change of the lateral displacement and the yaw angle. The results are listed in Table 2. When α_t increases from $\frac{1}{40}$ to $\frac{1}{20}$, the lateral displacement of the leading wheelset varies from −8.09 to −7.65 mm, and its yaw angle from 0.028° to 0.0345°. The longitudinal and lateral creepages of wheel 2 increase, respectively, from 0.00337 to 0.01103, and 6.04E-4 to 0.00206. They increase by more than 3 times. The lateral displacement of the trailing wheelset varies from −6.28 to −5.66 mm, and its yaw angle from −0.087° to −0.0749°. The absolute value of the lateral creepage of wheel 4 decreases by about 28%, and that of the longitudinal creepage increases about 60 times (from −1.12E−4 to 0.00709 shown in Table 2). The results shown in Fig. 21b suggest that the natural wear caused by the rolling contact of wheel and rail can efficiently increase by increasing the rail cant, which is beneficial to eliminating the existing small cracks or suppressing their growth rate on the rails.

The rail profile change, due to wear, depends not only on the wear volume along the rail running surface but also on the wear distribution on the rail top. Fig. 22 illustrates the distributions of the rail wear caused by the 4 wheels for $v = 120$ km/h, $h_t = 120$ mm and $\alpha_t = 1/20$. From Fig. 22, the wear volumes caused by wheels 2 and 4 on the low rail are much larger than those caused by wheels 1 and 3, but the widths of their distributions on the low rail top are relatively narrow. The density of the material removal caused by wheel 3 on the high rail is the lowest, but the lateral width of wear is the largest, compared with the other 3 wheels. The wear distribution width depends on the lateral width of the contact area, actually, depends mainly on the wheel/rail profiles at the contact point. At railway sites, if the wear occurring spreads over the rail top uniformly, the use life of the rail can be efficiently extended. At the sharp curved tracks of the heavy haul lines, actually, the severer wear concentrates on the inside corner of the high rail, as shown in Fig. 1a, and the uneven wear corrugates the running surfaces of the rails, as shown in Fig. 1b. The situation greatly reduces the curving behavior of the vehicle, and causes a strong vibration. So, controlling the rail wear is not only to control

the material removal from the rail but also to control its distribution on the rail top.

The wear changes the profiles of the wheel and the rail, and leads to the serious problems discussed above. But, the wear can efficiently eliminate small cracks on the rail running surface, and suppress the growth of the cracks. Based on the principle, railway companies scientifically grind the rails in service to relax the contact stresses, eliminate and reduce the rolling contact fatigue of the rails. By the grinding, the much changed profile of the rail is also renewed. Therefore, the material removal by grinding and its distribution on the rail top is a key technique in the grinding maintenance of track. With the increasing of the natural accumulated wear caused by the repeated rolling/sliding contact of wheel/rail, the continuous change of rail profile will lead to the change of the contact stresses. These are very important problems to be investigated further in the near future.

4. Conclusions

Some of the important published papers on wheel–rail wear are reviewed. Their studies are mainly based on laboratory experiments and numerical procedures. Wheel–rail wear study is a very complicated project involving many subjects and many factors some of which are stochastical. By test only, it is very difficult to identify various factors affecting the wear, and determine how much each factor contributes to the overall wear and the contact stress level. So far any advanced test facility can not represent track dynamic characters completely, such as non-linear damping and non-linear stiffness. So, it is very necessary and also important to develop the complete theoretical model to analyze the factors affecting the curved rail wear and the contact stresses. The present paper investigates the effect of the curving speed, the track super elevation and the rail cant on the rail wear at the curved track with a numerical method. The numerical results are concluded as follows:

(1) The difference between the normal loads of the left and right wheels of the wheelset increases quickly with increasing the curving speed. The curving behavior of the vehicle becomes more inferior, and the rail wear increases. But the variation of the maximum normal contact stress has a large fluctuation with increasing the curving speed due to the profiles of the wheel/rail. Namely, the change of the contact point position leads to the large change of the normal distance (or gap) between the wheel/rail. The normal distance is formed by the wheel/rail profiles. Therefore, the profiles of the wheel/rail dominate the maximum normal contact stress. So the improvement of the profiles is a key step in reducing the contact stress, but is complicated project.
(2) By increasing the super elevation of the curved track properly leads to the improvement of the curving behavior and the contact stresses, and the reduction of the rail wear.
(3) The rail cant has a great influence on the rail wear and the contact stresses. The change of the cant leads to the change of the motion status of the wheelset, such as the lateral displacement and the yaw angle of the wheelset, etc. A small change of the yaw angle can cause a large lateral creepage generation that will lead to the severe wear occurring on the rail running surface. In addition, changing the rail cant means turning the rail. The contact points on the wheel tread or the rail top shift sharply in the rail turning. In such a situation, the match of the wheel/rail profiles probably becomes more inferior or finer, which depends on the prescribed profiles. Hence, both the selection of the rail cant and the improvement of the wheel/rail profiles are simultaneously considered in the maintenance of the curved track.

Acknowledgements

The present work has been supported by the National Natural Science Foundation of China (50521503, 50675183), the National Basic Research Program of China (973 Program, 2007CB714702), and Specialized Research Fund for the Doctoral Program of Higher Education (20060613020).

The authors wish to express their many thanks to the reviewer and editors of the present paper. They gave very kind help in technique revising and English improvement of the paper.

References

[1] Clayton P. Predicting the wear of rails on curves from laboratory data. Wear 1995;181–183:11–9.
[2] Wen ZF, Jin XS, Zhang WH. Contact-impact stress analysis of rail joint region using the dynamic finite element method. Wear 2005;258:1301–9.
[3] Jergéus J, Odenmarck C, Lundén R, Sotkovszki P, Karlsson B, Gullers P. Full-scale railway wheel flat experiments. Proc Inst Mech Eng, Part F: J Rail Rapid Transit 1999;213:1–13.
[4] Kapoor A, Fletcher DI, Franklin FJ. The role of wear in enhancing rail life. In: Dowson D, et al., editors. Tribology research and design for engineering systems. Amsterdam: Elsevier B V; 2003. p. 331–40.
[5] Magel E, Roney M, Kalousek J, Sroba P. The blending of theory and practice in modern rail grinding. Fatigue Fract Eng Mater Struct 2003;26:921–9.
[6] Wu HM, Woody SS, Blank RW. Optimization of rail grinding on a North American Haul Railroad Line. In: Ronald J, Costa L., editors. Proceedings of the eighth international heavy haul conference. Brazil: 2005. p. 419–27.
[7] Ishida M, Abe N, Moto T. Experimental study on the effect of preventive grinding on RCF defects of Shikansen rails. In: Alexander L. Lisitsyn, editor. Proceedings of the IHHA'99 STS-conference. Masco: 1999. p. 511–6.
[8] Silva FCM, Vidon Jr W, Caldwell R. Preventive–Gradual on-cycle grinding: A first for MRS in Brazil. In: Ronald J, Costa L, editors. Proceedings of the eighth international heavy haul conference. Brazil: 2005. p. 435–45.
[9] Beagley TM. Severe wear of rolling/sliding contacts. Wear 1976;36:317–35.
[10] Bolton PJ, Clayton P, McEWEN IJ. Wear of rail and tire steels under rolling/skidding conditions. ASLE Trans 1980;25:17–24.
[11] Bolton PJ, Clayton P. Rolling-sliding wear damage in rail and tyre steels. Wear 1984;93:145–65.
[12] Fries RH, Dàvila CG. Analytical methods for wheel and rail wear prediction. In: Proceedings of the ninth IAVSD symposium, Linköping: 1985. p. 112–25.
[13] Tyfour WR, Beynon JH, Kapoor A. The steady state wear behavior of pearlitic rail steel under dry rolling-sliding contact conditions. Wear 1995;180:79–89.
[14] Muster H, Schmedders H, Wick K, Pradier H. Rail rolling contact fatigue. The performance of naturally hard and head-hardened rails in track. Wear 1996;191:54–64.
[15] Tournay HM, Mulder JM. The transition from the wear to the stress regime. Wear 1996;191:107–12.
[16] Ueda M, Uchino K, Kobayashi A. Effects of carbon content on wear property in pearlitic steels. Wear 2002;253:107–13.
[17] Deters L, Proksch M. Friction and testing of rail and wheel material. Wear 2005;258:981–91.
[18] Telliskivi T, Olofsson U. Wheel-rail wear simulation. Wear 2004;257:1145–53.
[19] Shen ZY, Hedrick JK. The influence of rail lubrication on freight car wheel/rail wear rates. In: Proceedings of the international conference on rail quality and maintenance for modern railway operation. The Netherlands: 1992. p. 523–35.
[20] Shen ZY, Hedrick JK, Elkins JA. A comparison of alternative creep-force models for rail vehicle dynamic analysis. In: Hedrick JK, editor. Proceedings of the 8th IAVSD Symposim. Lisse: Swets and Zeitlinger; 1984. p. 59–605.
[21] Jendel T. Prediction of wheel profile wear-comparisons with field measurements. Wear 2002;253:89–99.
[22] Archard JF. Contact and rubbing of flat surfaces. J Appl Phys 1953;24:981–8.
[23] Podra P, Andersson S. Wear simulation with the Winkler surface model. Wear 1997;207:79–85.
[24] Telliskivi T, Olofsson U. Simulation of wear in a rolling sliding contact by a semi-Winkler model and Archards wear law. Wear 2004;256:817–31.
[25] Telliskivi T, Olofsson U. Contact mechanics analysis of measured wheel-rail profiles using the finite element method. J Rail Rapid Transit 2000;215:65–72.
[26] Olofsson U, Telliskivi T. Wear, plastic deformation and friction of two rail steels—a full-scale test and a laboratory study. Wear 2003;254:80–93.
[27] Enblom R, Berg M. Simulation of railway wheel profile development due to wear-influence of disc braking and contact environment. Wear 2005;258:1055–63.
[28] Magel E, Kalousek J, Caldwell R. A numerical simulation of wheel wear. Wear 2005;258:1245–54.

[29] Shevtsov IY, Markine VL, Esveld C. Optimal design of wheel profile for railway vehicles. Wear 2005;258:1022–30.
[30] Kalker JJ. Three-dimensional elastic bodies in rolling contact. Dordrecht: Kluwer Academic Publishers; 1990. 137–84.
[31] Jin XS, Wen ZF, Zhang WH, Shen ZY. Numerical simulation of rail corrugation on curved track. Comput Struct 2005;83:2052–65.
[32] Bolton PJ, Clayton P, McEwan IJ. Rolling-sliding wear damage in rail and tyre steels. Wear 1987;120:145–65.
[33] Clayton P. Tribological aspects of wheel-rail contact: a review of recent experimental research. Wear 1996;191:170–83.
[34] Zhai WM, Cai CB, Guo SZ. Coupling model of vertical and lateral vehicle/track interactions. Vehicle Syst Dyn 1996;26:61–79.
[35] Jin XS, Wen ZF, Wang KY, Zhou ZR, Liu QY, Li CH. Three-dimensional train-track model for study of rail corrugation. J Sound Vib 2006;293(3–5): 830–55.
[36] Jin XS, Wen ZF, Wang KY, Xiao XB. Effect of passenger car curving on rail corrugation at a curved track. Wear 2006;260:619–33.
[37] Sato Y, Odaka T, Takai H. Theoretical analysis on vibration of ballasted track. Railway Technical Research Report, 1347 (1987).
[38] Zhai WM. Coupling dynamics of vehicle-track. Beijing: China Railway Press; 2001 (in Chinese).
[39] Zhai WM. Two simple fast integration methods for large-scale dynamic problems in engineering. Int J Numer Methods Eng 1996;39:4199–214.
[40] Igeland A, Ilias H. Rail head corrugation growth predictions based on non-linear high frequency vehicle/track interaction. Wear 1997;213:90–7.
[41] Knothe KL, Grassie SL. Modeling of railway track and vehicle/track interaction at high frequencies. Vehicle Syst Dyn 1993;22:209–62.
[42] Cai Z. Modelling of rail track dynamics and wheel/rail interaction. Ph.D. Thesis. Kingston, Ontario, Canada: Queen's University; 1992.
[43] Grassie SL, Gregory RW, Harrison D, Johnson KL. The dynamic response of railway track to high frequency vertical/1ateral/1ongitudinal excitation. J Mech Eng Sci 1982;24:77–102.
[44] Thompson DJ, Jones CJC. A review of the modelling of wheel/rail noise generation. J Sound Vib 2000;231:519–36.
[45] Damme S, Nackenhorst U, Wetzel A, Zastrau BW. On numerical analysis of the wheel-rail system in rolling contact. In: Proceedings of colloquium on system dynamics and long-term behavior of railway vehicles, track and subgrade, May 2002, Stuttgard, Germany, p. 155–74.